FABRICATION AND TESTING OF A MICRO-SCALABLE PH SENSOR FOR IMPLANTED BIOMEDICAL USE

by

Elias T. Hilliard

B.S. in Mechanical Engineering, University of Pittsburgh, 2007

Submitted to the Graduate Faculty of

the Swanson School of Engineering in partial fulfillment

of the requirements for the degree of

Master of Science in Mechanical Engineering

University of Pittsburgh

2010

UNIVERSITY OF PITTSBURGH

SWANSON SCHOOL OF ENGINEERING

This thesis was presented

by

Elias T. Hilliard

It was defended on

August 19, 2009

and approved by

Dr. William W. Clark, Professor, Mechanical Engineering Department

Dr. Sung Kwon Cho, Associate Professor, Mechanical Engineering Department

Dr. Minhee Yun, Assistant Professor, Electrical Engineering Department

Thesis Advisors: Dr. William W. Clark, Professor, Mechanical Engineering Department,

Dr. Sung Kwon Cho, Associate Professor, Mechanical Engineering Department

FABRICATION AND TESTING OF A MICRO-SCALABLE PH SENSOR FOR IMPLANTED BIOMEDICAL USE

Elias T. Hilliard, M.S.

University of Pittsburgh, 2010

Biosensors have recently moved into the arena of implantable devices. This incredible capability, to continuously monitor physiological parameters in-situ, allows for earlier and fundamentally more accurate measurements. As pH is one of the most important biological factors, implantable devices to measure pH are of great interest. Unfortunately, current pH sensors exhibit signal drift and require regular recalibration. Since this is impractical for implanted devices, much work is needed in order to extend the working life of the pH sensor. The present work implemented three techniques for fabricating a pH sensor based on an iridium oxide sensing layer that are compatible with micro-fabrication techniques and implantable devices. They are the oxidation of pure iridium, reactive sputtering of iridium in an oxygen environment, and anodic electrodeposition of iridium oxide. The response of the sensors based on these indicating layers to tests in buffer solution revealed a high degree of linearity. Slopes of the response were in agreement with those found in the literature. Life tests were performed to characterize the signal drift over 20 hours of continuous use. The established processes for fabricating the pH sensors provide a vehicle for further investigation into techniques for extending life, specifically, by using microfluidic devices. Preliminary tests were done to show that interruption of the electrochemical circuit slows signal drift. This can be accomplished in microscale devices using a microfluidic switching mechanism proposed here.

Keywords: pH sensor, iridium oxide, signal drift, EWOD, microfluidics.

TABLE OF CONTENTS

PREFACE viii

1.0 INTRODUCTION AND LITERATURE REVIEW 1

1.1 Definition of pH 2

1.2 Nernst Equation 2

1.3 Importance of pH Measurements 4

1.4 Current Macro-scale pH sensors 5

1.5 Motivation 6

1.6 Microscale Advantages 7

1.7 The Reference Electrode 8

1.7.1 Electrical reference point 8

1.7.2 Real reference electrodes 9

1.8 The Indicating Electrode 11

1.8.1 The ISFET 11

1.8.2 Metal oxides 11

1.8.2.1 Oxidized iridium 12

1.8.2.2 Sputtered IrO_2 12

1.8.2.3 AEIROF 13

1.9 Switching Mechanism 14

2.0 EXPERIMENTAL FABRICATION PROCEDURES 17

2.1 Oxidation of Iridium Wire 17

2.2 Sputtered Iridium Oxide 18

2.3 Electrodeposition of Iridium Oxide on Titanium 19

2.4 Silver-Silver Chloride Electrode Fabrication 21
2.5 Experimental Setup and Data Acquisition 22
3.0 EXPERIMENTAL RESULTS 25
3.1 Linearity of Sensor Response 25
3.1.1 Response for the Three Electrode Types 25
3.1.2 The AEIROF Response 27
3.2 Porcine Blood Test 29
3.3 Lifetime of Sensors 30
3.4 Preliminary Tests of Switching 36
3.5 Response Time 40
4.0 CONCLUSION 43
4.1 Summary of Results 43
4.2 Future Work 44
BIBLIOGRAPHY 46

LIST OF TABLES

1 List of Materials and Reagents 24

2 pH Sensor response to pH for IrO_2 electrode types 26

3 Response of AEIROF electrodes due to storage condition and Nafion® coating. . . 28

4 Post-blood test calibration 30

LIST OF FIGURES

1 Standard Macro-scale pH sensor 6
2 Bubble movement caused by EWOD 15
3 Design of Switching Mechanism 16
4 Sputtered Electrodes Sketch 19
5 AEIROF on Bulk Ti 21
6 Diagram of Electrodes in Measurement Setup 23
7 Diagram of Data Acquisition System 24
8 pH Response 26
9 AEIROF storage conditions 28
10 Lifetimes of 3 types of IrO_2 Sensors 31
11 Sputtered IrO_2 Lifetime 32
12 Oxidized Ir Wire After Decay 33
13 Sputtered Life Test with Changing components 33
14 Experimental Setup for Switching Simulation 38
15 Dip Test 1 39
16 Dip Test 2 40
17 AEIROF Response Times 42

PREFACE

First and foremost I would like to acknowledge Dr. William Clark and Dr. Sung Kwon Cho, who have been exemplary advisors and have earned my gratitude and respect both personally and professionally. Next, I would like to acknowledge the University of Pittsburgh's Office of Technology Management and Dr. Marco Zenati who have financially supported this project.

I would like to thank all those who have additionally contributed to my success in this endeavour. I would especially like to thank Yushin Kim, as well as Kathy Davis, and Yifan Tang, fellow graduate students at Pitt in the Chemistry Department whose selfless spirit of collaboration caused them to give of their time and effort in order to assist me in my research, receiving no personal reward for themselves. I would also like thank Dr. Shigeru Amemiya who gave me invaluable advice and access to his equipment, and Dr. Alexander Star who also allowed me to use his laboratory resources. These persons are testaments to the spirit of collaboration and integrity at Pitt that make me proud to be an alumnus.

Finally, I would like to thank those in my personal life who have encouraged me and brought me to this point: my siblings– Simon, Justine, Reuben, and Hadassah; my mother and stepfather, whose expressions of pride and support have been a source of motivation; and my late father, a man who I will always hold in utmost regard. I would also like to thank my high school mentors, Mr. Shane Cornwell and Mr. Timoty Wollein, who have continued to support me through all these years.

1.0 INTRODUCTION AND LITERATURE REVIEW

The importance of hydrogen ions, H^+, has been known since the start of last century, and measurement of its presence is one of the most common tasks performed in the chemistry lab today. As a result, pH sensors are widely available with features for a variety of applications. As with any sensor there is still error to reduce and shortfalls to accommodate, so pH sensor design and optimization continues with an expectant clientele.

Recently the Food and Drug Administration has approved the use of some micro-electromechanical systems (MEMS) for permanent implantable sensing. So far, these sensors are used for non-invasive monitoring of physiological parameters in patients with abdominal aortic aneurysms and heart failure. This has opened the door for researchers in the MEMS field to expand applications for their devices. In particular, continuous monitoring of pH is of interest. pH is of significant importance to human health, and it may be used for early detection of potentially serious conditions, as will be discussed. Unfortunately, classic pH sensors are incompatible with long term in-vivo measurements. The reasons for this are two-fold. First, the indicating electrode is made of ion-sensitive glass which (i) is too large for micro-scale applications and (ii) could break, spilling solution internally and exposing tissue to sharp edges. Second, pH sensors exhibit regular signal drift. For this reason regular recalibration is required, which is not usually possible for long term in-vivo measurements.

Much research has been done in the field of chemistry in order to resolve these problems. This work developed a pH sensor that is microscalable and suitable for implantable devices. This sensor is intended to be a vehicle for investigation of extending sensor life with mechanical options, specifically, by means of a microfluidic switching mechanism. Motivation is further discussed in Section 1.5. Because this thesis crosses multiple disciplines which the reader may not be familiar with, some introductory material is presented for review.

1.1 Definition of pH

S. P. L. Sørenson originally defined pH in 1909. His definition, which is still commonly taught in introductory chemistry courses, is based on the molar concentration of H^+, denoted H^+ in Eq. 1.1. It is given by

$$pH = -\log\left(H^+\right) \tag{1.1}$$

[10]. However, technical difficulties quickly arise with this definition, as it only holds for ideal solutions and strict equality of the liquid junction potentials, and it relies on an inaccurate definition of ion concentration [5]. This has resulted in the use of the nomenclature, psH ('s' for Sørenson) for the definition given in Eq. 1.1 [5]. Current practice and theory uses a similar definition based on the *activity* of the hydrogen ions. "[T]he activity of a single ionic species is a concept lacking unique physical definition" [5], but it represents the fraction of ions which contribute to reactions. While rigorous thermodynamic definitions exist, it is sufficient for the present discussion to recognize that values for this "effective concentration" can be determined experimentally. The original definition of pH persists because, commonly, an appreciation of acidity and alkalinity can be gained by relative comparison of pH values, and rigorous calculation is unnecessary [10]. Further, in practice, measurements of pH are made relative to buffer solutions, rather than directly measuring H^+ activity. Thus, evaluation of the alkalinity or acidity of a solution is based on a comparison scale. In summary, it is acceptable to think of pH as a measure of H^+ concentration because pH is a relative scale, and activity and concentration are closely related (so much so that they are often used interchangeably, though imprecisely) so that a change in true pH is equal to a change in psH [5].

1.2 Nernst Equation

The Nernst Equation, given by

$$E = E^\circ - \frac{RT}{nF}\ln(a_{red}/a_{ox}) \tag{1.2}$$

predicts the electric potential of an oxidation-reduction (redox) reaction based on the activity ratio of the reducing and oxidizing agents, a_{red}/a_{ox}. The potential, E, of the cell is offset by E°, the potential of the cell at standard, reference conditions. R and F are constants, n is the number of electrons transferred, and T is temperature in degrees Kelvin.

Since hydrogen ions are strong oxidizers, their activity is readily detectable. In the electrochemical cell, they interact with available negative ions on the sensing electrode, and a charge accumulates according to the Nernst Equation. The activity of those ions remains constant between measurements, but the activity of H^+, of course, does not. Therefore the charge on a sensing electrode changes only with the activity of the H^+ at a given temperature. From Eq. 1.2, it follows that a change in pH is proportional to the change in electric potential of the electrochemical cell. Further, since the pH scale is determined by the use of buffer solutions, as discussed earlier, it is reasonable to calibrate a pH sensor's output curve, a straight line, using buffer solutions. Thus we use the Nernst Equation to identify that E is a linear function of pH, and buffer solutions to determine the slope and offset of that curve. The pH of a test solution can then be determined by interpolation/extrapolation. Mathematically,

$$
\begin{aligned}
E \quad &= E^\circ - \tfrac{RT}{nF}\ln(a_{red}/a_{ox}) \\
&= E^\circ - C_0\ln(a_{red}/a_{H^+}) \qquad = E^\circ - C_0\ln(a_{red}) + C_0\ln(a_{H^+}) \\
&= C_1 + C_0\log(a_{H^+})/\log(e) \quad = C_1 + C_2\log(a_{H^+}) \\
&= C_1 - C_2\cdot pH
\end{aligned}
$$

and values of C_1 and C_2 are determined by calibration.

Therefore, a pH sensor consists of an electrode sensitive to the activity of H^+ according to the Nernst Equation, connected (via a salt bridge) to an electrode with a stable reference potential, both incorporated into a proper data acquisition and readout mechanism. The necessity of the second electrode is explained in Section 1.7. There are other pH indicators such as color changing dyes and test papers [5], but these are of no concern to this study.

1.3 Importance of pH Measurements

In his papers, Sørenson described the importance of the hydrogen ion to cell life; an identification which has only been strengthened since the publications. Water is the solvent in all cells and intracellular fluids, and in order to dissolve organic compounds, water dissociates into H^+ and OH^- ions. The concentrations of these ions, and therefore pH, effect the behavior and concentrations of other ions in and around cells, such as the ammonium ion (NH_4^+) and the carboxyl group (—COOH) frequently found on organic molecules [34, 2]. Accordingly, the pH of a biological system is an important factor in the regulation of the rates at which chemical processes occur. Cells have several mechanisms for maintaining cytosolic pH around the optimum value, 7.40, because small deviations from this value can have profound consequences on the rate of cell metabolism [34]. Understanding and measuring cell pH is vital for the study of the most fundamental forms of life.

Further, measurement of pH is extensively used as a diagnostic tool in the medical field. Measuring a patient's blood pH for acidosis or alkalosis can provide "an important clue to doctors that a serious problem exists" [6]. Blood pH is controlled by the respiratory and the renal systems. Therefore, a disease of the respiratory system, such as emphysema, chronic bronchitis, or pulmonary edema would result in respiratory acidosis. Similarly, poorly controlled type I diabetes mellitus, an abnormal metabolism, or advanced stages of shock, for example, would cause metabolic acidosis. Finding a pH value greater than normal, over 7.45, would indicate alkalosis, suggesting possibilities such as an overactive adrenal gland, the use of diuretics, or it may be the result of hyperventilation due to anxiety or cirrhosis of the liver [6, 52].

Besides its relevance in the circulatory system, acidity is important in the digestive track. The digestive processes use strong acids to break down food. Failure of the stomach lining or lower esophageal sphincter to protect the stomach or esophagus from these acids results in peptic disorders like gastritis, peptic ulcers, and gastroesophageal reflux disease. While it is true that doctors do not usually require pH tests for diagnosis [6], these conditions are caused by stomach acid imbalances. Naturally, research into the fluctuations in acid levels requires close monitoring of stomach and esophagus pH levels [29, 28, 24].

Finally, pH is monitored in a variety of non-biological/-physiological circumstances such as rainwater and environmental studies [22], drinking water monitoring [1], soil monitoring [42, 19], sewage treatment, industrial waste, and various industrial processes.

As a result of the wide variety of situations where pH plays an important factor, there exists a need for pH sensors that can withstand a wide variety of environments. A universal pH sensor would need to withstand high temperatures, corrosive environments, and wide pressure ranges, as well as require only small test samples, have a fast response time, exhibit low signal drift, and have high sensitivity, all over a long lifetime.

1.4 Current Macro-scale pH sensors

The industry standard pH sensor is a combination reference electrode and indicating electrode housed in a single probe (see Figure 1C). The reference electrode is usually either the saturated calomel electrode (SCE) or the silver-silver chloride (Ag/AgCl) reference electrode, Figure 1B, and has a reference element in a solution of constant ionic strength, the inner electrolyte. (Technically speaking, the "reference electrode" is a reference half-cell, as described [38]. For the sake of clarity and familiarity, this paper uses the term "reference electrode" as is common among the literature, and adopts Midgley and Torrance's [38] practice of referring to the actual reference electrode as the "reference element".) This is electrically connected through a porous, typically ceramic, plug to the test solution. The indicating electrode, Figure 1A, is also in the test solution and is based around a H^+ sensitive glass bulb. The response of the glass is transmitted via another electrolyte to a reference element inside the glass housing (which incorporates the ion sensitive bulb and contains the electrolyte). With a pH meter connected to the leads of each electrode, the electrochemical circuit is complete. The individual electrodes and the combination are illustrated in Figure 1. The electric potential generated across the electrodes is read by the pH meter and converted into pH units. The pH meter must have an extremely high input impedance, on the order of 10^{12} Ω or higher, due to the high output impedance typical of the sensor. The voltage-to-pH conversion algorithm is based on the Nernst equation and user-established calibration points.

Many manufacturers offer access for refilling electrolytes, and most pH sensors also include a temperature compensation feature, since E is dependent on temperature, as Eq. 1.2 describes.

While the standard pH sensor has been well established, the drive toward smaller technology has found it lacking. Specifically, the H^+ sensitive glass bulb does not lend itself to micromanufacturing technologies, and a remodel is in the works. Some research has attempted to change the entire setup, but as far as the reference electrode is concerned, the most successful changes are primarily in scale and geometry, not in operational theory. On the other hand the pH sensitive electrode, as will be discussed, has seen some interesting new directions.

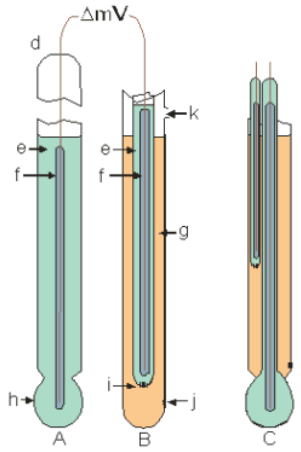

Figure 1: Macroscale pH electrode. (A) Indicating Electrode (B) Reference Electrode (C) Combination Electrode, A+B. (d) seal (e) internal filling solution (f) internal reference electrode (g) external filling solution (h) pH-sensitive glass membrane (i) internal liquid junction (j) external liquid junction (k) fill hole. (Picture taken from Thermo Orion website http://stu.inonu.edu.tr/~e982527)

1.5 Motivation

Because pH sensors are subject to signal drift they require regular calibration. While this does not present a problem for most lab measurements and individual sample tests, applications which require continuous monitoring, implantable devices for example, are limited. Some research has

been done to automatically recalibrate sensors [7], or to compensate for the signal change [20] in order to circumvent this problem, but most work has been done on extending the stable period of the sensor. Extending the sensor life is an unending investigation into the improvements of materials, geometries, configurations, and fabrication techniques. Researchers have incorporated hydrogel electrolytes, ion-selective polymers, field-effect transistors (FETs), metal oxides, specialized chemical growth geometries, sputtering techniques, electron-beam evaporation, electrodeposition, and chemical oxidation to name a few examples. The novelty of the microfluidic switching device is that it can be applied to existing and new configurations, multiplying any improvements made by research on the *chemistry* of pH sensing. This is because the switching mechanism allows the pH sensor to be turned on and off (see Section 1.9) effectively pausing the use, and therefore decay, of the pH sensors. Assuming that life span is linearly related to use time, turning the sensor off for 90% of the time could cause a ten-fold increase in life span. A low-duty cycle is particularly suited for infrequent, short duration sampling. A pH sensor with a fast response, completing a measurement in 10 sec for example, and a long lifetime, 100 hr of continuous use, could be used to sample pH once an hour for over 4 years! Of course, this estimation is an idealization and assumes that turning off the sensor will stop all signal decay, which may not be reasonable. While this concept makes sense in principle, experimental verification is necessary.

One application which has particularly driven this study is the implantable pH sensor for myocardial (heart) tissue pH monitoring. Ischemia, the restriction of blood supply (and therefore oxygen) in blood vessels, has been shown to be strongly correlated with a drop in myocardial pH [4]. As ischemia is a precursor to myocardial infarction (heart attack), early detection can allow for preventative action to be taken and lives to be saved. In consideration of this application, a test of the developed pH sensor in porcine blood was tested and is discussed in Section 3.2.

1.6 Microscale Advantages

Much work has been done in the development of micro-scale electrodes for pH sensing. Micromanufactured pH sensors have several advantages over traditional glass electrodes. As with most MEMS devices, the batch processing dramatically reduces cost of fabrication, smaller devices re-

quire less material, and downstream costs, such as packaging and shipping, are lower as well. As mentioned, a micro-pH sensor which does not incorporate glass components can be made flexible and virtually unbreakable, which is of particular interest for in-vivo measurements. Perhaps the most significant advantage is that micro-scale electrodes also have the ability to measure smaller quantities and may be able to operate in spatially confined environments. Finally, reduced cost and size in microscale biomedical applications often allows for the devices to be disposable, simplifying or eliminating sterilization issues. Of course the transition to microscale is not without its difficulties, and the work toward an optimal microscale pH sensor is underway across a variety of avenues.

1.7 The Reference Electrode

1.7.1 Electrical reference point

As with any voltage measurement, the potential at a point in the electrochemical circuit is measured with reference to some other point in the circuit. No assessment of the absolute number of electrons is made, only the difference between two charges is measured. In order to create a constant reference charge, against which an indicating electrode's charge can be measured, a reference electrode is incorporated. Ideally, the reference electrode maintains a constant charge while allowing for electrical connection in any test solution. The charge on the indicating electrode changes with the variable under measurement. The potential on the indicating electrode is measured against the reference point and any change in it is interpreted as a change in the variable of interest. Clearly then, the performance of the reference electrode is exactly as important as that of the indicating electrode.

Since this is true of all electrode systems, the question arises: How can comparisons be made between dissimilar reference electrodes? That is, if the reference point changes between tests, how can two tests be compared? Some universal reference point is needed. This point is the charge on the standard hydrogen electrode (SHE), which has an electric potential of identically 0 V by convention. Using this reference an electric potential can be determined for any reaction.

Thus using a SHE as a reference electrode, and a known value of E°, the Nernst Equation can be used to calculate the activity in a redox reaction from a measured electric potential. In practice, superior reference electrodes, such as the Ag/AgCl reference electrode or the SCE, which have known potentials, can be used. Their offset from zero (the SHE potential) is used to adjust the calculation. As an example, consider the case of the Ag/AgCl reference element in a solution containing chlorine ions (Cl^{-}), and at standard conditions. The Cl^{-} in solution exchange with the dissociated AgCl. The concentration of ions around the AgCl surface generates a charge at the electrode. This is the charge calculated by the Nernst Equation and is based on ion activity. In this example, the charge generated at the AgCl surface is 222 mV stronger than the charge at the SHE. Thus, the potential of an Ag/AgCl electrode is 222 mV (referenced to the SHE by convention) [26]. Now any reaction's electric potential can be measured against a Ag/AgCl reference electrode. If an output of 100 mV is observed, then we know the reaction has a potential of 322 mV vs SHE.

1.7.2 Real reference electrodes

Because reference electrodes contain an inner solution and must make electrical contact with the test solution, there exists some interface between the two. Ideally, this interface would have no electric potential, and retard mass transfer between the solutions perfectly. One way to achieve the first condition is to use a free-diffusion liquid junction. This junction allows the inner electrolyte to diffuse into the test solution, creating a direct, "electrically shorted" connection [15, 16]. Inconveniently, mass transfer is restricted only by limiting the area of the interface between solution volumes. In time, the inner electrolyte will mix with the test solution, and the reference element will not maintain a constant reference potential. This problem makes miniaturization of a free-diffusion junction virtually impossible, as the small quantity of inner electrolyte will rapidly mix with the test solution, changing the reference potential. This can be solved by continuously refreshing the inner electrolyte, but that requires a constant supply to be pumped through.

The common solution is to limit mass transfer by using a solid liquid junction. This junction is porous for electrical connections and therefore, still allows the slow leaching of ions. Unfortunately, the liquid junction also has a nominal electrical resistance which causes a small electric potential drop across the liquid junction. The practice of making pH measurements based on buffer

solutions can accommodate this potential, if it is invariant, by simply adding it to the charge associated with the reference element. That is, the reference charge is considered the sum of the charge of the reference element and the liquid junction's potential. The potential of the electrode system is calibrated with buffer solutions, and the effect of the liquid junction potential is then nullified. However, concerns have been raised that the liquid junction's potential is not invariant across test solutions [25]. A difference in ionic composition of test solutions can translate into different liquid junction potentials. This would mean that the reference electrode, as well as the indicating electrode, are changing the electric potential measured; the first changes with ion concentration of the test solution, the other with the variable of interest, e.g. pH. The measurement is no longer isolated to the effects of the variable of interest. Despite acknowledging these concerns, Suzuki and co-workers use a solid liquid junction [48] in reported results. Subsequent authors have both followed and ignored the recommendations of Covington [7, 23, 46], who prescribed the use of a free-diffusion liquid junction as a standard for pH measurement. It is therefore unclear the extent to which variations in the liquid junction potential is of practical concern. This study has also disregarded this concern with the justification that, if necessary, calibration could be done in solutions with ion strength similar to that of the test solution.

The excellent operating characteristics of the macro-scale Ag/AgCl reference electrode, such as its very high exchange-current density reactions [26, 27], as well its compatibility with microfabrication techniques [49] make it a natural choice for miniaturization. However, problems arise during the transition to the micro-scale; significantly, the solubility of AgCl which becomes nontrivial when the AgCl layer is so small [49]. Numerous authors have already addressed this problem with various improvements which have extended the working life of the miniature Ag/AgCl reference electrode from a few minutes to several hours [31, 39, 3, 40]. Another problem results from the small quantity of inner electrolyte available in a miniature reference electrode. The porosity of the liquid junction allows mass transfer across it. Thus, the inner electrolyte leaches into the test solution or vice versa, and over time, the charge on the reference element drifts [48].

1.8 The Indicating Electrode

Two of the most popular candidates for the indicating electrode of a micro-scale pH sensor are the ion-selective field effect transistor (ISFET) [47] and metal oxide electrodes [31, 18]. The ISFET is batch fabricated like any electronic element of similar complexity and design. This means that a well established micromachining procedure and the means to achieve it, are necessary. On the other hand, metal oxide electrodes can be formed by a variety of chemical means and are essentially a single compound on a substrate. So the metal oxide electrodes lend themselves to simple lab fabrication and testing much more so than the ISFETs. In light of this and the high recommendations made by several authors, the metal oxide electrode was chosen early on for investigation and will therefore be the focus of this thesis.

1.8.1 The ISFET

The ISFET is part of a solid-state integrated circuit. As such, it can be batch fabricated in silicon with planar integrated circuit technology which has been well established for many years. This allows the potential for the integration into microchips capable of on-chip signal processing [47]. One of the first noted operating characteristics of the ISFET is its extremely fast response time, which is on the order of 1 millisecond [51]. This effectively eliminates the acquisition time for any pH measurement, allowing immediate detection of changes in pH. They are also quite rugged – suitable for in-vivo applications [47].

1.8.2 Metal oxides

Among metal oxides, iridium oxide has received significant attention because of its wide pH response range, high sensitivity, fast response time, low potential drift, insensitivity to stirring, wide temperature and pressure operating ranges, and low sensitivity to redox pair interference [36]. An iridium oxide layer can be achieved via a variety of techniques including: electrochemical oxidation via potential cycling, reactive sputtering, anodic electrodeposition, and thermal oxidation, among others [18].

1.8.2.1 Oxidized iridium The simplest means of creating iridium oxide is to oxidize a pure iridium wire by means of potential cycling. Using an iridium base guarantees good charge communication between the base and the sensing layer, and eliminates concern over unwanted oxidation of the base metal. Numerous authors have accomplished fabrication of the electrode by cycling in dilute acid, typically sulfuric acid (H_2SO_4) [9, 21, 41]. Parameters such as the precise acid concentration, voltage range, cycling speeds, number of cycles, and pre-/post-cycling recipes, vary from author to author. These parameters lead to various interpretations of the exact structure of the iridium oxide, but there is general consensus that the sensitive layer formed is IrO_2. Without any additional features, the Ir/IrO_2 electrode has shown reasonable pH sensing behavior. Some authors [9, 21] found that an initial aging of their electrodes in either distilled water for a month or in buffer solution of pH 4.01 for 12 hours, could decrease the amount of drift to various degrees. This aging period may be causing changes in the oxide film stoichiometry that results in a more uniform film [21]. Regardless of the aging protocal, the electrode potential responds linearly with pH and is steady to within a few millivolts, in some cases for up to 100 hours of operation. Response time has been shown to be less than 1 second [9, 21, 41]. There is strong agreement across the research that IrO_2 exhibits a super-Nernstian response. That is, the sensitivity of the pH sensor is greater than the $|-59|$ mV/pH unit (at 25 °C) which the Nernst equation predicts [5]; it is typically around -75 mV/pH unit. The mechanism for this may still be up for debate, but the effect is of minor importance, and higher sensitivity is an advantage in sensors.

1.8.2.2 Sputtered IrO_2 Iridium oxide has been sputter deposited [44] and shown to be sensitive to pH [30]. In these cases the oxide is created by sputtering Ir in an oxygen environment, where it reacts to form IrO_x and is thus called *reactive sputtering*. Sputtering has several advantages over oxidation techniques including: (i) batch fabrication is easier to implement, (ii) direct deposition gives the flexibility necessary for multi-probe manufacture, and (iii) there is no constraint to use iridium as a substrate [30]. The behavior of the sputtered IrO_2 electrode under various stimuli such as prolonged exposure to air/pure water at normal/elevated temperatures/pressures has been researched by several groups. It has proven to be rather robust. The response curve showed only minor deviations in the slope, which is near-Nernstian [32, 50], in contrast to the oxidized or electrodeposited films. The environment has also shown changes in the linear offset (i.e. E°, in Eq.

1.2). These deviations could also be accounted by calibrating the sensor in a similar environment. (If this sort of calibration is not possible, post-processing of the signal may be required.)

Aging has also been reported [30, 32, 50, 33]. Experiments have shown that the surface undergoes hydration over the course of about 24 hours. After this time an offset of several hundred millivolts is seen on the pH-response curve. Because the mechanism of hydration leaves the IrO_2 intact, the effect can be reversed by simply drying the electrode [33]. This suggests that the sputtered IrO_2 electrode could be (i) stored in air at all times, and used for brief measurements (since the time constant of hydration is so long), or (ii) stored in solution for 24+ hours before its first use and at all times after (in order to maintain the hydrated response curve, which is still linear).

In contradiction to Marzouk's claim of low sensitivity to redox species, Kinlen *et. al.* found that there was appreciable output interference [31]. Nafion® was therefore suggested to protect against redox pairs, but its inclusion comes at a cost of lengthening the response time. Without the coating, response was nearly instantaneous, but once protected, Nafion® can increase the response to well over a minute. The response time also becomes somehow pH dependent, being worst around the neutral pH range, and faster at extreme pH values [31].

1.8.2.3 AEIROF Anodically electrodeposited iridium oxide films (AEIROFs) have the advantages of allowing for planar fabrication while eliminating need for expensive iridium targets. Further, electrodeposition techniques do not require high temperature techniques which may be inappropriate for some desired flexible (polymer-based) substrates [36]. Since being introduced by Yamanaka [53], the procedure for the producing AEIROFs has been significantly improved [35]. Platinum had been previously used as a substrate, but due to poor adhesion, was not reproducible. A study on the choice of substrate was performed, and it was determined that titanium was superior to several other pure metals and metal alloys. Development time of the electrodeposition solution has been shortened so that complete electrode fabrication can take less than an hour. However, recommendation is made to immerse the electrode for 2 days in order to reduce the potential drift to acceptable levels. The AEIROFs also exhibit a super-Nernstian response typically with a slope in the range of 60-75 mV/pH. Marzouk reported a trade-off between protection from redox species with Nafion® and lengthened response time that was similar to Kinlen's findings.

Iridium oxide boasts numerous impressive qualities, and is available via a variety of techniques. Oxidizing Ir substrates is the easiest way to create IrO_2, but it requires the use of solid Ir, which is expensive. Sputter deposition requires an expensive Ir target, but it can be spread a long way and on a variety of substrates. It also allows for batch fabrication, a must for commercial production of micro-electrodes. Lastly, AEIROFs seem to have all the benefits of sputter deposition, without the cost of Ir targets. Research has revealed, however, that the fast response time boasted by all IrO_2 electrodes is negated by the necessity of a protective coating.

1.9 Switching Mechanism

The use of microfluidics to turn on and off a microscale pH sensor has been proposed as a means of extending sensor life. The pH sensor developed in this research has been used to investigate the plausibility of this concept. Extensive work has been done here at the University of Pittsburgh's Mechanical Engineering and Materials Science Department under the direction of Dr. Sung Kwon Cho on the manipulation of bubbles in μ-liter volumes (e.g. [54, 55, 12, 13]). Bubble movement in 2D via sequential activation of electrode pads has been thoroughly described and demonstrated [11, 55], as well as all practical concerns such as bubble generation and elimination related to manipulation devices [14]. Thus collaboration with Dr. Cho and researchers will allow for expert fabrication of a switching mechanism via bubble transportation. The switching mechanism will use the electrowetting on dielectric (EWOD) principle to move a bubble through a channel. The principle is as follows. A bubble in solution will change contact angles when an electric potential is applied across the solution. If the contact angle is changed asymmetrically, the deformation causes a pressure difference inside the bubble, giving rise to bulk fluid movement [11], as illustrated in Figure 2. Sequential deformation and movement of the bubble results in a controllable transportation.

This ability to manipulate bubbles can be used to move an air bubble over the liquid junction, interrupting the electrical connection. This "turns off" the the pH sensor without having to remove it, so that the sensor is preserved while sampling is not being performed. If this stops all signal drift, this would theoretically extend the life of the sensor by a factor inversely proportional to

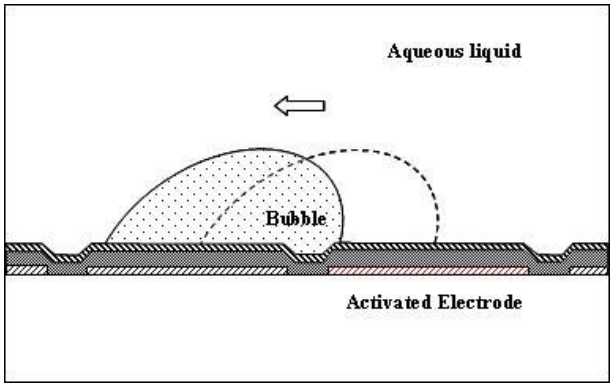

Figure 2: Activating the electrode on the right causes asymetric deformation of the bubble and a net force on the bubble which pushes the bubble away from the activated electrode. (Picture courtesy of Sang Kug Chung.)

the fraction of time it is turned on. Since an electric potential, which may interfere with signal readings, is used to manipulate the bubbles, a master-slave bubble relationship was devised as seen in Figure 3. This allows for movement of the slave bubble without direct stimulation.

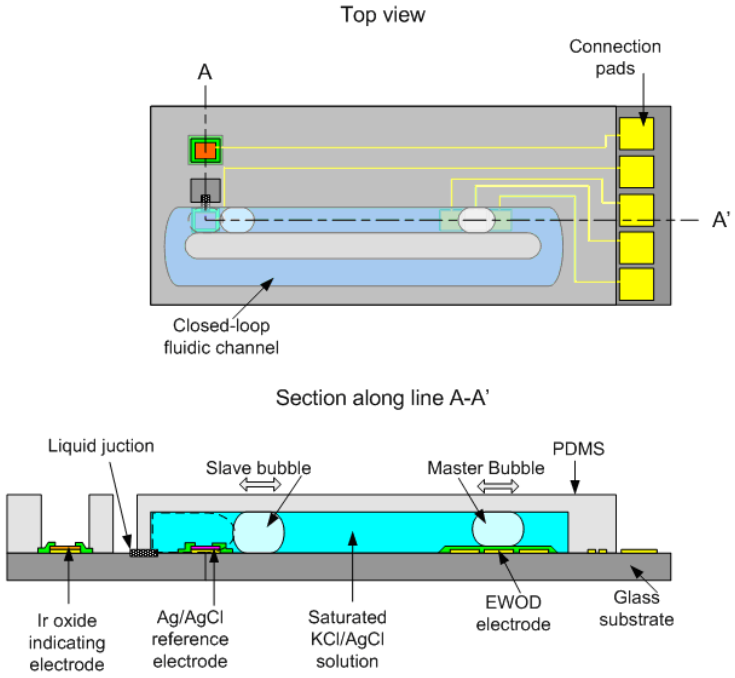

Figure 3: Proposed design for a micro-scale pH sensor with a novel switching mechanism for extended life. EWOD manipulation of master bubble will drive movement of slave bubble to interrupt cicuit.

2.0 EXPERIMENTAL FABRICATION PROCEDURES

For the reasons described, iridium-oxide was chosen early on as the ion sensitive material. The three methods of electrode fabrication described in Section 1.8.2, were examined. All of these techniques can be incorporated into a micro-manufacturing process. The goal of this work was to establish capability to fabricate a pH sensor for use in in-vivo testing, and provide evidence that inclusion of a switching mechanism would increase the lifespan of similar pH sensors. The following sections describe the procedure for fabrication of the three types of indicating electrodes. Materials and reagents used are summarized in Table 1. All voltage measurements in this chapter are made vs. a Ag/AgCl reference electrode made by CH Instruments (CHI111).

2.1 Oxidation of Iridium Wire

Numerous authors have investigated the oxidation of an iridium wire using potential cycling [8, 9, 43, 21, 41]. Following the work of Hitchman and Ramanathan [21] a 1.0 mm diameter iridium wire was cycled between -0.20 V and 1.30 V in 0.5 M H_2SO_4 several thousand times at a rate of 3 V/s. At this rate one full cycle was completed every second. Since every cycle consisted of a potential sweep from one extreme end of the range to the other, and then a sweep back to the beginning, the Ir wire was oxidized and then reduced each cycle. This caused formation and destruction of the IrO_2 layer each cycle. As the number of completed cycles increased, the oxide that was formed each cycle thickened. This was seen by the color of the blue oxide which darkened as cycling progressed, so that eventually a dark blue layer of IrO_2 was visibly flashing on and off the Ir wire with a 1 Hz frequency. In order to end the cycling process at the appropriate stage of oxidation, the last cycling was performed at 0.030 V/s, giving time to accurately interrupt the cycle at the peak

of oxidation. Typically the IrO_2 film covered approximately 1 cm of the end of the wire. The wire was prepared for oxidation by cleaning with fine polishing papers, beginning with a 30 μm grit and decreasing grain size down to 15, 9, 3, 2, and finally, 1 μm. After polishing with paper, the electrode was polished with metallurgical techniques using a slurry of 0.05 μm alumina particles. After metallurgic polishing the wire was sonicated for 45 min in de-ionized (DI) water, changing the water every 15 min and rinsing with more DI water. As the last step was difficult to perform on a small wire, and it seemed to be excessive to polish with such fine particles, its omission was attempted. However, excluding this step caused the oxidation to fail. Evidently, either the fine polishing or the extensive sonicating played a critical role in electrode preparation. (Sonication is a process in which an object is submerged in solution which is being agitated at frequencies in or above the audible range. In this case it was done for cleaning purposes.)

2.2 Sputtered Iridium Oxide

Owing to the cost of purchasing an Ir target and the difficulty of *reactive* sputtering, the sputtered IrO_2 was purchased from a third party, rather than being fabricated in-house. A 15.24 cm (6") diameter wafer of reactively sputtered IrO_2 was purchased from MicroConnex (Snoqualmie, WA, USA). The product is described as pure Si with 2,000–3,000 Å gold (Au) (adhesive layer) plus 1–1.5 μm Ir-oxide. The wafer was cut into squares approximately 1 cm x 1 cm. There was no electrical continuity between the backside and IrO_2 surface. So, for electrical connection, the IrO_2 and Au layers were ground away in one corner, and a copper wire was soldered to the exposed Si substrate. A nylon based nail polish was used to insulate the connection as well as the back and sides of the thin square electrode. An ohmmeter was used to verify electrical connection between lead and sensing surface. For the tests of Figure 16, described in Section 3.4 only, the sputtered samples were prepared without attaching leads. These electrodes were larger than the other sputtered electrode samples, about 1 cm x 4 cm. For this reason alligator clips could be clipped directly onto the electrode without attaching leads. The IrO_2 surface was made discontinuous between the submerged surface and the electrical connection by cutting through the IrO_2 with a Dremel tool.

Again, the sides and back of the electrode were insulated with nylon based nail polish in order to block any unwanted electrical pathways. Sketches of these electrodes are shown in Figure 4.

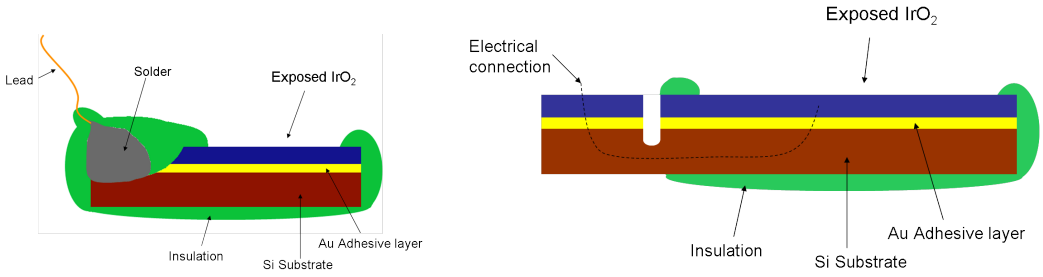

Figure 4: Sketch of cross sections of (left) smaller 1x1cm sputtered electrode and (right) larger 1x4cm sputtered electrode.

2.3 Electrodeposition of Iridium Oxide on Titanium

After reviewing several approaches to fabricating IrO_2 electrochemically, the procedure outlined by S. A. M. Marzouk [35] promised to be the superior technique for the project. The work done by Marzouk and his predecessors on AEIROF fabrication has been optimized to provide (i) excellent adhesion of IrO_2 to substrate, (ii) excellent reproducibility, (iii) faster preparation procedure, and (iv) an inexpensive choice of substrate (Ti compared to, e.g. platinum (Pt)) [35].

The electrodeposition solution was developed by dissolving 75 mg of iridium(IV)chloride hydrate ($IrCl_4{\cdot}xH_2O$) in 50 mL of DI water. A 500 µL aliquot of hydrogen peroxide (H_2O_2) was added followed by 365 mg of potassium oxalate monohydrate ($C_2K_2O_4{\cdot}H_2O$), stirring for approximately 10 minutes between addition of each reagent. Potassium carbonate (CO_3K_2) was added in small increments until the pH of the solution reached 10.5. After thorough mixing of all reagents, the solution was heated using a hot plate. The prescribed heating procedure called for heating the solution at 80°C for 10 min while monitoring with a thermometer. This was said to be sufficient to turn the solution dark blue, a necessary condition for proper electrodeposition. Since the volume of the solution was only 50 mL, no thermometer was available for such small volumes and accurate measurements of the solution temperature was not possible. In addition, it was this experimenter's

experience that it took longer than 10 min for the solution to turn dark blue. This may be because Marzouk's report oversimplified the heating procedure, or because the experimenter used a lower heat setting to warm the solution to temperature. Heating of the solution over 100°C was avoided with caution as Marzouk expressed concern that boiling the solution may have detrimental effects on the electrodeposition solution, such as decomposition of the oxalate. After the solution turned dark blue, heat was removed and the solution was allowed to return to room temperature. The solution was stored in a refrigerator and used for up to three weeks after fabrication.

Titanium substrates were prepared in two ways. Thin-film Ti was used to establish that Marzouk's technique could be used for microfabrication. A thin Ti layer, ≈100 nm, was sputter deposited onto glass. The Ti surface was roughened by immersing it in >51% H_2SO_4 at 80 °C for 1 min. Electrodeposition was performed via bulk electrolysis with coulometry (BEC) in the developed solution for 5 min at 1.0 V (vs Ag/AgCl). Longer roughening periods would cause complete dissolution of the thin Ti layer. Hastelloy gauze was used as a counter electrode. Exposed surface area was approximately 2.5 cm x 2.5 cm. The IrO_2 surface was greenish-blue in color, as predicted by Marzouk, and a cursory test of the electrode's response to pH was performed and was shown to be linear. These two indicators suggest that the electrode was successfully created on thin-film Ti. Once the possibility of the microfabrication of IrO_2 on a sputtered thin film was confirmed, bulk Ti substrates were used for convenience.

Bulk titanium substrates were made from 2.0 mm diameter rods cut to 2–5 cm in length. One end, the surface to be electroded, was ground flat then smoothed with sandpaper and polished with polishing papers as was performed on the Ir wire in Section 2.1. The surface was also roughened in hot H_2SO_4 but for much longer, typically 3–5 min, as there was no danger of dissolving away all the Ti substrate. Prior to electrodeposition the sides of the Ti rod were insulated with nylon based nail polish so that the exposed surface area was limited to the end of the rod. A small portion of the opposite end of the rod was left uninsulated for electrical connection, as seen in Figure 5. As a galvanostat, which was preferred over the BEC technique, became available, bulk Ti electrodeposition was performed via chronopotentiometry. Marzouk recommended using a constant current density of 2.0 mA/cm for 2.5 min. This recommendation corresponded to a current setting of 6.3×10^{-5} A for the 0.031 cm^2 geometric surface area described. However, in practice it was found that this was inadequate to deposit a visible IrO_2 layer. In order to determine a sufficient

current a cyclic voltammogram (CV) was generated by sweeping over a range, typically between 0.0 and 1.0 V. A local maximum current was found from the anodic peak in the CV. This current was then used to deposit IrO_2 for several minutes at a time. The color, uniformity and coverage of the deposit was checked between deposition attempts, and deposition times were adjusted as seemed fitting. Deposition was stopped when a continuous dark blue layer covered the entire exposed surface similar to the electrode shown in Figure 5, which is an excellent example of IrO_2 electrodeposition. Commonly, the total deposition time was 10–30 min, but some depositions took as long as 1.5 hrs. The variety in deposition current and times is attributed to a learning curve associated with developing a procedure for deposition. Some variability is no doubt due to minor differences in electrode surface preparation, and insulation, which controlled the surface area. For specified samples, Nafion® coating was added by dipping the electrode in 5 wt% Nafion® and air-drying twice.

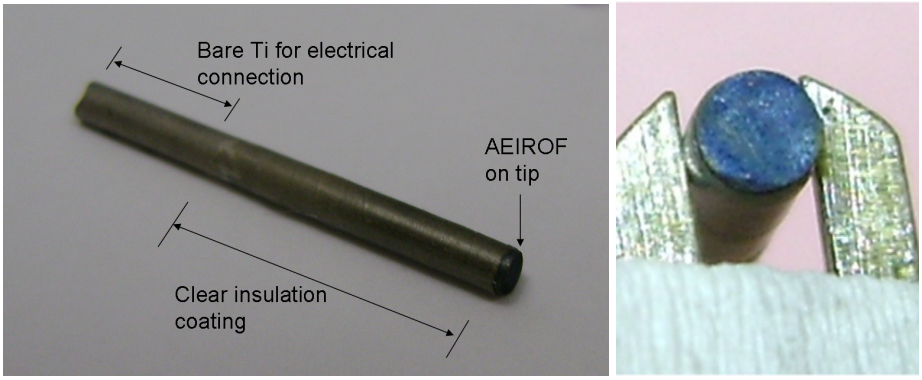

Figure 5: AEIROF electrode fabricated as described in Section 2.3. Figure shows (left) entire electrode and (right) tip of electrode being held by tweezers.

2.4 Silver-Silver Chloride Electrode Fabrication

Attempts were made to produce a Ag/AgCl reference electrode using micro-manufacturing techniques. Silver was sputter deposited directly on glass slides and with various adhesive layers including chromium (Cr), Ti, and Au/Cr. During chloridization of the Ag or testing of the Ag/AgCl

layer, the Ag consistently peeled off. Despite changes to Ag and adhesive layer thicknesses, as well as trying different chloridization techniques, the Ag was repeatedly lost. As the adhesion of Ag to a proper substrate is certainly achievable, it is assumed that the author's inexperience in micro-manufacturing and chemical techniques was at fault. Improvement of the Ag adhesion was postponed indefinitely, and bulk Ag techniques were taken up.

The Ag/AgCl reference element was fabricated by applying 0.3 V across a 0.5 mm diameter pure Ag wire in saturated KCl for 60–70 s. A Pt wire was used as a counter electrode. When not in use, the Ag/AgCl reference elements were stored in a solution of saturated KCl and AgCl, which was also used as the inner electrolyte of the completed reference electrode.

2.5 Experimental Setup and Data Acquisition

To create the reference electrode, the Ag/AgCl element was submerged in saturated KCl and AgCl held by a small vessel. The housing vessel was machined in-house out of acrylic in the shape depicted in Figure 6. Porous vycor tips, manufactured by Bioanalytical Systems Inc. were used for the liquid junction, which was secured to a hollow stem machined into the acrylic vessel by heat shrink tubing supplied with the vycor tips. The setup is shown in Figure 6. This configuration was used in order to facilitate changing of the inner electrolyte and to accommodate larger electrodes that were to have been made on glass substrates via micro-manufacturing techniques.

Due to the high output impedance of pH sensors, and in order to minimize unwanted current flow, the input impedance of the data acquisition (DAQ) system must be extremely high. To address that issue, an operational amplifier (op-amp) with an input impedance on the order of 10^{14} Ω specifically for pH probes was used (Model AD795, Analog Devices). Unless otherwise specified, this amplifier was wired as a non-inverting op-amp with a gain of $G = 1 + \frac{R_f}{R_{gnd}} = 1 + 2\text{k}\Omega/1\text{k}\Omega = 3$, as shown in Figure 7. The output of the circuit was divided by the gain before being reported. Thus the true output of the sensor is reported throughout. It may be helpful to note for other investigators, that the choice of amplification circuit is critical. When wired as a differential amplifier, the IrO_2 was lost, presumably dissolved into the solution through unintended reduction. Evidently, the reference electrode must be tied to ground. Similarly, not using high impedance device as

recommended will cause a decay in the indicating electrode and a corresponding drop in output. The amplified signal was sent to a National Instruments (NI) Input/Output box, NI USB-6008, which transmitted the signal to a personal computer. Data processing and storage was done by NI's LabVIEW 8.0 software. The author wrote LabVIEW code to sample the input voltage at user defined intervals and save the time and voltage data to a spreadsheet, where post-processing could be performed. A diagram of the DAQ system is given in Figure 7.

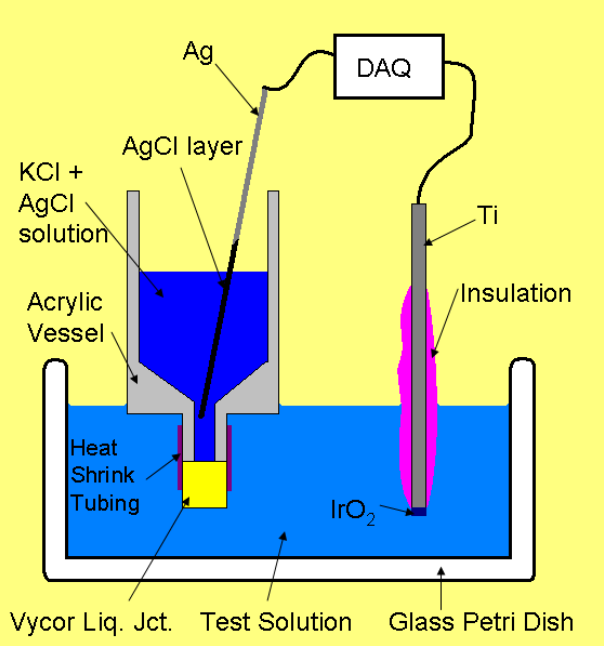

Figure 6: Cross-section: Reference electrode and AEIROF-based indicating electrode in measurement setup.

Measurements were taken by arranging the electrodes and DAQ system as shown in Figure 6. Electrodes and glassware were rinsed with DI water between all measurements. Unless otherwise noted, the test solutions were universal buffer solutions of pH 4 (Biphthalate), 7 (Phosphate), or 10 (Borate) ±0.01 pH units at 25 °C manufactured by J. T. Baker.

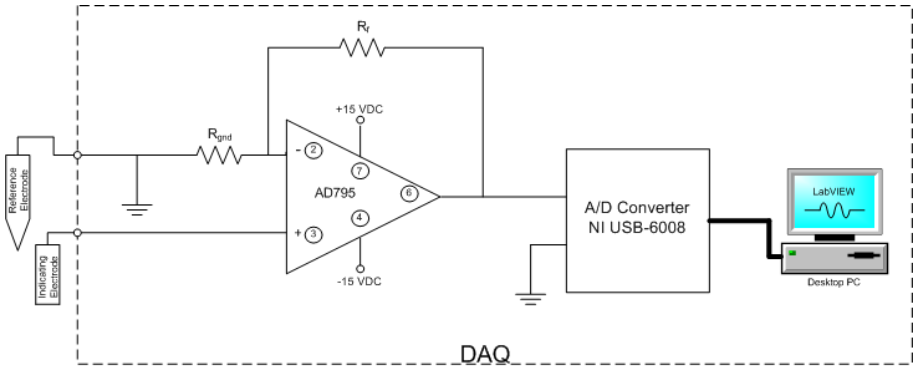

Figure 7: Data Acquisition System

Table 1: List of Materials and Reagents

Item	Vendor	Item or Stock #	Description
Ir wire	Alfa Aesar	11429	1.0 mm dia., 99.8% pure
Polishing Papers	3M	–	Six grades: 30, 15, 9, 3, 2, and 1 μm grit
$IrCl_4{\cdot}xH_2O$	Alfa Aesar	12184	99.95% (metals basis), Ir 56.5% min
$C_2K_2O_4{\cdot}H_2O$	Fisher Scientific	AC424025000	99%
CO_3K_2	Fisher Scientific	AC424085000	
Hastelloy C gauze	Alfa Aesar	40938	20 mesh woven from 0.23 mm dia wire
Pt wire	Alfa Aesar	45093	0.25 mm dia, 99.9% (metals basis)
Ti wire	Alfa Aesar	10397	99.7% (metals basis)
Ag wire	Alfa Aesar	11433	0.5 mm dia., 99.9% (metals basis)
KCl	J. T. Baker	–	
AgCl	Fisher Scientific	AC21127-0100	99+%
Vycor Tips	Fisher Scientific	50854579	3.5 mm dia. x ≈4.3 mm

3.0 EXPERIMENTAL RESULTS

This chapter will present the results of various experiments performed in order to characterize the quality of the fabricated electrodes. In addition, evidence is provided that microfluidic switching is likely to slow signal drift. All long duration (1 hour or more) tests were performed using the lab-made reference electrode as described in Section 2.4 Figure 6. This was done in order to control the concentration of the inner electrolyte between tests, and to avoid rapid wear of the commercial electrode. For all other tests, i.e. pH response and response time tests, a commercial Ag/AgCl reference electrode from CH Instruments (CHI111) was used. Long duration tests were performed in pH 7 buffer solution.

3.1 Linearity of Sensor Response

3.1.1 Response for the Three Electrode Types

Measurements of the IrO_2 electrodes' output showed excellent linearity with respect to pH. Tests were performed by measuring the indicating electrode's electric potential with respect to a commercial Ag/AgCl reference electrode in various pH buffer solutions as described in the preceding chapter. The output at each pH is given for the three types of indicating electrodes in Table 2 and graphed in Figure 8, including an AEIROF on thin-film Ti. The slope and intercept of a line through these points were determined from a linear regression analysis, and are given along with the square of the correlation coefficient, R, to assess the quality of the fit. Being very near to 1, this value indicates an excellent fit for each of the sensors.

Table 2: pH Sensor response to pH for IrO_2 electrode types

Type of IrO_2 electrode	pH 4	pH 7	pH 10	Slope	Offset	R^2
Oxidized Ir wire	0.748 V	0.520 V	0.303 V	-74.1 mV/pH	1.042 V	0.9998
Sputter deposited IrO_2	0.460 V	0.299 V	0.155 V	-50.9 mV/pH	0.6609 V	0.9989
AEIROF on thin-film Ti	0.62 V	0.37 V	0.16 V	-76.7 mV/pH	0.920 V	0.9975
AEIROF on bulk Ti	0.327 V	0.124 V	-0.108 V	-72.5 mV/pH	0.6218 V	0.9986

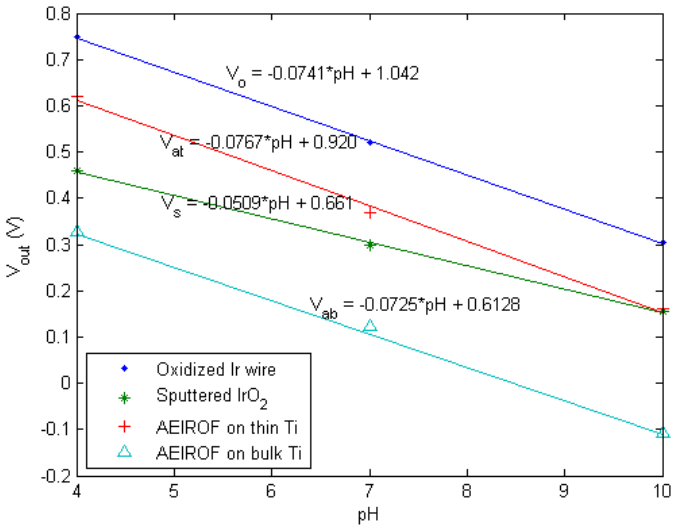

Figure 8: Response of pH sensors to buffer solutions.

Details of the measurements were as follows. The test on the electrode with a thin-film Ti substrate was performed prior to acquiring a proper DAQ system. For this reason, only peak values were taken over brief sampling times. It was later found that the proper DAQ system prevented the decay as discussed in Section 2.5, but it is reasonable to assume that the peak response is an accurate indication of the electrode's response to pH, based on the linearity of the results and agreement of the slope with results reported elsewhere. For the other tests, the electrode potential was measured over a few minutes and many data points, 50+, were averaged to minimize random error. The standard deviation in each of these measurements was always very small, being less than 4 mV and none more than 2% of its respective average. The oxidized wire response was measured using a CH Instruments 660 Electrochemical Analyzer in Open Circuit Potential – Time mode. The other two tests were performed as described in Section 2.5, with a commercial Ag/AgCl reference electrode.

From Table 2 it is clear that the electrochemical techniques produced electrodes with super-Nernstian responses, while the sputter deposited electrode has a sensitivity much closer to the Nernst Equation prediction. These results are in agreement with the research discussed previously, in Section 1.8.

3.1.2 The AEIROF Response

Since the AEIROF is the superior choice of electrode fabrication technique (see Section 1.8), further investigation on electrodes of this type was performed during the course of the research. Marzouk recommended storing the electrodes made of AEIROF on Ti in a buffer solution of pH 7. The author's experience was that this caused the blue deposit, which was indicative of a well developed IrO_2 film [35], to fade visibly, as seen in the comparison in Figure 9. For this reason, a comparison was made between the response of electrodes stored in air, and those stored in pH 7 buffer solution. These data are given in Table 3. Included in the table are electrodes with and without the Nafion® coating recommended by references [31, 35]. The electrodes are identified by storage and coating as AU: stored in Air, no Nafion® (Uncoated); AC: stored in Air, Nafion® Coated; BU: stored in Buffer solution, Uncoated; and BC: stored in Buffer solution, Nafion® Coated.

Figure 9: AEIROF electrodes on left have been stored in pH 7 buffer solution, while electrodes on right have been stored in air. Clearly the buffer solution storage has caused fading of blue iridium-oxide deposit, which is at the bottom of Ti rods.

Table 3: Response of AEIROF electrodes due to storage condition and Nafion® coating.

Electrode	pH 4	pH 7	pH 10	Slope	Offset	R^2	Blood pH
AU	0.232 V	0.019 V	-0.112 V	-57.3 mV/pH	0.448 V	0.9811	7.99
AC	0.288 V	0.092 V	-0.110 V	-66.3 mV/pH	0.554 V	0.9999	6.23
BU	0.085 V	-0.077 V	-0.267 V	-58.7 mV/pH	0.324 V	0.9981	7.24
BC	0.091 V	-0.165 V	-0.272 V	-60.4 mV/pH	0.308 V	0.9465	6.63
Average	–	–	–	-60.7 mV/pH	0.408 V	0.9814	7.02

Interestingly, the slopes of each of these curves are slightly lower than expected. In fact, the output of the electrode stored in air without Nafion® coating (AU) was the same electrode reported in Table 2. The only significant difference between measurements is the time after fabrication at which the measurements were taken. After several weeks in storage, the electrodes have aged in such a way that they are less sensitive to pH, and still exhibit a linear response. The aging seems to be independent of storage conditions. This is also indication that changes in the reference electrode are not the only source of drift that will eventually need to be addressed. As this issue was discovered unintentionally and late in the research, its cause and characteristics have been left open for investigation.

3.2 Porcine Blood Test

As a practical example of the ability of the pH sensor to measure pH in an implanted environment, the sensor response in a sample of porcine (pig) blood was measured. A small quantity (≈5 mL) of heparinized porcine blood was provided from a live pig undergoing surgery. Measurements of pH were made using a commercial Ag/AgCl reference electrode, and each of each of the electrodes in Table 3. The output was recorded with a Tektronix TDS2014B Digital Oscilloscope for more than 30 seconds. Five hundred data points were averaged, and the result was used to calculate the pH values given in the last column of Table 3 using the slope and offset presented in the same table. The average of the sample set is also given, the pH reading for which was 7.02 with a standard deviation of 0.765. For comparison, a Heska i-Stat handheld clinical analyzer was used to measure the pH. According to this commercial sensor, the blood pH was 7.37. A reasonable standard for error in a pH sensor is +/- 0.1 pH units, or +/- 0.01 for precise laboratory or medical uses. Assuming that the commercial blood analyzer was accurate, the prototype electrodes showed unacceptable amounts of imprecision by this standard. This is not surprising for a first attempt at fabricating a pH sensor by this research group. It suffices to know that the sensor is responding properly to H^+ activity, and further improvements to the electrodes would improve the precision of the sensor.

Table 4: Response of AEIROF electrodes after blood tests.

Electrode	pH 4	pH 7	pH 10	Slope	Offset	R^2	Blood pH
AU	0.269 V	0.080 V	-0.128 V	-66.3 mV/pH	0.537 V	0.9993	7.73
AC	0.184 V	0.048 V	-0.125 V	-51.7 mV/pH	0.396 V	0.9952	5.92
BU	0.107 V	-0.051 V	-0.251 V	-59.7 mV/pH	0.352 V	0.9953	7.58
BC	0.141 V	-0.013 V	-0.205 V	-57.7 mV/pH	0.379 V	0.9961	8.18
Average	–	–	–	-58.8 mV/pH	0.416 V	0.9965	7.36

After the test was completed, a post-test calibration was performed to determine whether or not the blood environment had changed the sensor. The results of this test are given in Table 4. The average slope and offset for the four electrodes were -58.8 mV/pH and 0.416 V, respectively, and the standard deviations were 6.0 mV and 0.083 V. Had the post-test calibration curves been used to measure pH, the average, which was 7.36, would have been much closer to the blood analyzer's measurement, but the spread in the data was even larger, the standard deviation being 0.99 pH units. The Nafion® coating did not play a distinguishing role in any of the data gathered from these tests.

3.3 Lifetime of Sensors

Since a critical issue under investigation is the signal drift of the sensor output, a survey of the electrodes was done to examine the output over an extended period of time, 20+ hours of continuous use. Figure 10 shows the change in output of the pH sensor for each of the three indicating electrode types. The oxidized Ir wire shows a drift of about 1 mV/hr. The sputtered samples showed a non-linear change in output, changing about 28 mV in the first 8 hours, and then less than 7 mV in the following 12 hours. The AEIROF indicating electrode showed a similar nonlinear decay, however in this case the magnitude of the signal decreased, moving in the opposite direction at nearly the exact same rate. Since the reference electrode was the same across these tests, it must

be concluded that the indicating electrode plays a role in the drift of the sensor output. This does not necessarily indicate that mere exposure to the test solution is the cause of the decay. During the course of the research many tests were done prior to acquiring a suitable DAQ system. The output of the system consistently resembled a negative exponential, as does the AEIROF response in Figure 10. In the earlier tests, however, the decay was much more rapid, easily 100 times faster. This suggests that the increased input impedance, by reducing current flow, greatly magnifies the time constant of the IrO_2 decay. If the current that flows through the electrochemical cell, allowing for measurement of the electrochemical potential, also causes the decay of the IrO_2 electrode, then opening the circuit by means of a switching mechanism, like the one discussed in Section 1.9, would stop the current flow, halting the decay of the indicating electrode.

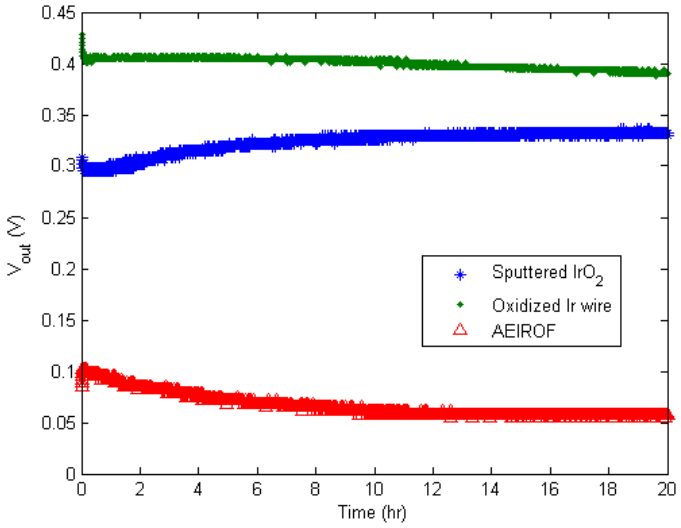

Figure 10: Lifetimes of sensors made with the three types of fabrication techniques.

That hypothesis seems to conflict with the results of the following, repeated life tests. A life test on a sputtered electrode was performed and then repeated four days later with the same indicating electrode and fresh reference electrode components. The graphs of these tests are shown in Figure 11. First, it is noted that there appears to be an offset change in the output between the two tests. This might suggest a permanent decrease in potential on the IrO_2 electrode was caused by the first test, however subsequent tests did not show this to be a trend. It is reasonable to suggest that the offset is associated with random differences in the reference electrode between tests. The

second characteristic of Figure 11 to notice is the fact that the second test started at essentially the same point, as opposed to near where the first test ended. This suggests that the near exponential change in the output is related to the reference electrode in some way, and not to the current flow through the electrochemical cell as hypothesized in the preceding paragraph. If it were, the decayed indicating electrode would not return to near its initial output, it would have already undergone the change, and would, presumably, continue from that point.

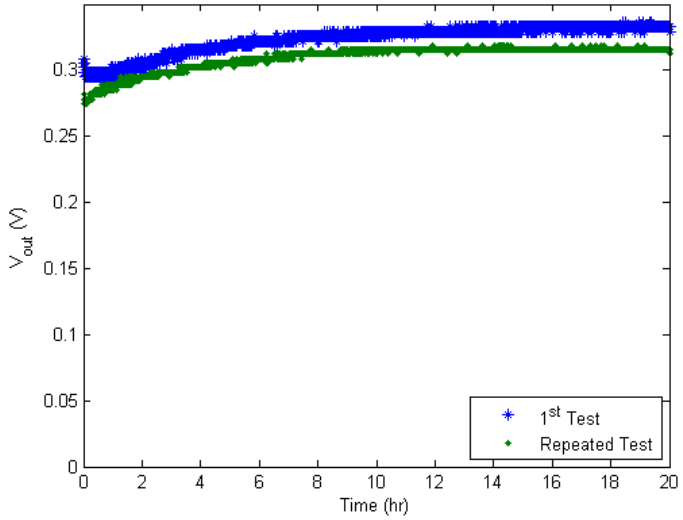

Figure 11: Output of Sputtered IrO_2 and Ag/AgCl electrode over a 20 hour period. Test was repeated after replacing the inner electrolyte and the reference element to show that changes in these were cause of quick, nonlinear drift.

There is, however, at least one explanation that allows for the hypothesis to be maintained in light of the results of the repeated life test. The possibility is that after the IrO_2 is damaged by the current flow, the time stored in air between tests, which was four days in the case presented, somehow reverses these effects. The damaged IrO_2 was reoxidized. While it may seem unlikely that the electrode "repaired itself", this happened to both the oxidized Ir wire and the AEIROF electrodes. These types of electrodes underwent life tests, and when the output rapidly decayed, the blue iridium oxide had disappeared to the naked eye. A photo of an oxidized Ir wire at this stage is shown in Figure 12. After a day of exposure to air, the surface of the Ir or Ti had regained the blue color where it had been lost, and was again sensitive to pH.

Figure 12: Oxidized Ir wire showing loss of IrO_2 due to testing without proper DAQ system. After storage in air, end of Ir wire which had been previously oxidized fully regained its bluish-purple color.

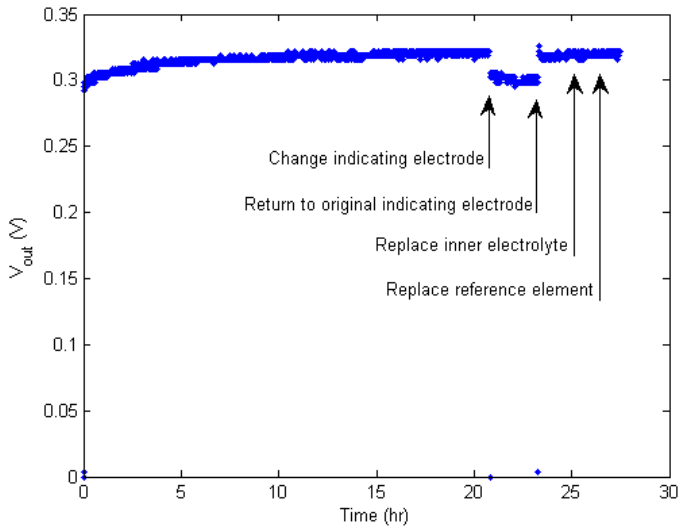

Figure 13: Life Test on a sputtered IrO_2 electrode during which the indicating electrode, inner electrolyte, and reference element are all changed in order to see which one "resets" test to state of pre-exponential decay.

In order to further investigate the cause of the exponential decay, an experiment was run, during which all components of the electrochemical cell were replaced with fresh components. This was done one at a time, in order to isolate each variable. It was hypothesized that replacing the responsible component would cause the total electrochemical cell to return to its pre-exponential decay state, and then repeat the decay as that component aged. The test proceeded as described by Figure 13. First, the potential of a sputtered IrO_2 electrode was measured against a reference electrode for over 20 hours. Then the indicating electrode was replaced with a different electrode of the same type, which had been stored in air. The second electrode had a potential of about 17 mV less than what the original electrode had been outputting prior to the switch. This, as can be seen from Figure 13, was actually quite close to the initial output of the original indicating electrode; however, after 2.4 hr the output remained constant at that value. This suggested that the difference in output was due to random difference between the indicating electrodes, not trends characteristic of the electrodes. That is, this change in output was an offset difference, not a resetting of the electrochemical cell. In pH sensing, it is typically the relative potentials that are of concern, so difference in the absolute offset of the two electrodes was ignored. At this point, the original indicating electrode was returned since it was apparently not the cause of the exponential decay. This was done in order to minimize variables in the tests to follow. After reestablishing the conditions of the first 20 hours of testing, the inner electrolyte was replaced, and then, more than an hour later, the Ag/AgCl reference element was replaced. No change in the output was observed after either of these changes. Thus the indicating electrode, inner electrolyte, and reference element had been eliminated as causes of the exponential decay. Finally, an experiment was devised to determine if properties of the liquid junction were causing the signal drift. While in storage, the liquid junction was submerged in saturated KCl, the inner electrolyte. If the ionic content of the porous liquid junction affected the liquid junction potential, which was discussed in Section 1.7.2, then it would be conceivable that this content was changing over several hours, since it was newly exposed, on one side, to the test solution at the start of the test. As the ions in the test solution began to permeate the liquid junction, the liquid junction potential would approach an equilibrium which reflected the potential due to a steady-state mix of K^+, Cl^- ions and test solution ions. In order to test this hypothesis, the liquid junction was stored in the test solution in order to cause a complete permeation of the liquid junction with test solution ions. A positive test would be one in which

the electric potential of the total system started above the steady-state potential, and decreased to that equilibrium position. This did not happen. The test proceeded as the previous life tests had, indicating that the liquid junction was not a factor in the exponential decay.

These tests suggest that the cause of the exponential decay is more complicated than the case of one component decaying due to extended use. The decay is apparently due to a combination of elements in the total electrochemical cell being active over an extended period of time. This is further suggestion that a properly executed switching mechanism could interrupt the decay and extend the life of the pH sensor. Of course further investigation and an explanation of the underlying chemical principles would be needed to complete the analysis begun here.

In addition to this study, an analytical investigation into the effect of ions leaching from the reference electrode was performed. The inner electrolyte and liquid junction in contact with a test solution were modeled as a finite volume of solution with concentration, C_0, separated from an infinite solution of zero concentration, by Vycor glass (the liquid junction) with thickness, L. Diffusion of the solute across the Vycor is descibed by Fick's Second Law, the diffusion equation, more commonly recognized as the Heat Equation, given by

$$\frac{\partial C}{\partial t} = D\frac{\partial^2 C}{\partial x^2} \tag{3.1}$$

which can be solved for the finite system using the separation of variables technique [45]. The most general form of the solution is then

$$C(x,t) = \sum_{n=0}^{\infty} \left[A_n \cos \lambda_n x + B_n \sin \lambda_n x\right] e^{-D\lambda_n^2 t} \tag{3.2}$$

In order to determine a unique solution, two boundary conditions and one initial condition are needed. Since the liquid junction was stored in the inner electrolyte before testing, the initial condition, $C(x,0) = C_0$, was used. Since the approximation of infinite solvent on the test solution side, at $x = 0$, was made, an appropriate boundary condition would be $C(0,t) = 0$ for $t > 0$. The second boundary condition used was of *the Third Kind*, also called a *Robin Boundary Condition*, given by $\frac{\partial C}{\partial x}|_{x=L} = -\alpha C(L,t)$. This boundary condition states that the flux into the liquid junction

is proportional to the concentration at that surface. These boundary conditions result in the Sturm-Liouville problem [37]. Applying the first boundary condition gives $A_n = 0$ for all n. Applying the second boundary condition results in the solution set for λ_n, in terms of α:

$$\tan \lambda_n L = \frac{-\lambda_n}{\alpha} \tag{3.3}$$

and the solution

$$C(x,t) = \sum_{n=1}^{\infty} B_n e^{-D\lambda_n^2 t} \sin \lambda_n x \tag{3.4}$$

The term, B_n is determined from the intial condition, and when substituted into Equation 3.4, gives the total solution [37]:

$$C(x,t) = 2\alpha \sum_{n=1}^{\infty} \frac{1 - \cos \lambda_n L}{\lambda_n(\alpha L + \cos^2 \lambda_n L)} e^{-D\lambda_n^2 t} \sin \lambda_n x \tag{3.5}$$

Of interest in this solution is the time constant, τ, which describes the time it would take for ion leaching through the liquid junction to contribute to a change in the solution concentration. From Equation 3.5 this is given by $\tau^{-1} = D\lambda_n^2$. From the literature [17], a reasonable approximation of the diffusion coefficient is $D = 3{\times}10^{-8}$ cm^2 s^{-1}. While an approximation of α is not readily available from the literature, an examination of Equation 3.3 reveals a narrow range for the first approximation (n=1) of λ_1. For any $\alpha > 0$, and $L = 0.5$ cm, $\pi \leq |\lambda_1| \geq 2\pi$. Thus, 235 hr $< \tau <$ 938 hr. Thus, the fastest approximation of the time constant resulting from Equation 3.5 is 235 hr, which is much slower than the drift observed. This suggests that signal drift due to the leaching of ions through the liquid junction is not a dominating factor in this study.

3.4 Preliminary Tests of Switching

The aforementioned LabVIEW program was modified to include motor control which was used to dip the reference electrode into and remove it from the test solution. “Motor engage” and “motor direction” signals were sent to an H-bridge which controlled a LEGO® motor. The motor moved a rack and pinion attached to the reference electrode. Motor actuation caused the reference electrode

tip to be submerged or removed from test solution as appropriate, thus simulating the "on" and "off" settings by closing and opening the electrochemical circuit. Figure 14 is a photograph of the setup. "On" and "off" intervals were determined by user input. Of course, voltage readings taken while the sensor is in the "off" state reflect ungrounded/unreferenced voltage measurements, and are thus nonsense. This simulates an interruption of the electrochemical circuit but is an imperfect simulation of the setup described in Section 1.9 in two obvious ways. First, the circuit described in Figure 3 places the air interruption between the inner electrolyte and the liquid junction. In the performed experiments, the interruption happens on the opposite side of the liquid junction, between it and the test solution. This difference allows for discrepancies in the way the liquid junction and its associated electric potential behave. Second, the air bubble in the final micro-scale design is of finite volume, and a very small volume at that, on the order of a few μL. Compare this to the virtually infinite volume of an open room, which cannot be saturated with ions that escape from solution, nor will it be exhausted of ions that dissolve into the solution from atmosphere. In addition, the volume of inner electrolyte in the prototype reference electrode is much larger than in the microfluidic system. Therefore, any effects of aging influenced by the volume, such as leaching of ions through the liquid junction, may be severely mitigated.

Two sets of tests were performed on sputtered IrO_2 electrodes. First, the sputtered electrode used for the life test in the preceding section was used in a dip-test for 11 hours. The electrode was submerged in the test solution for 10 s intervals, and then removed for 10 s. Since the submerged portion simulates the time during which the sensor is "on", this tests represents a scenario when the sensor is on half the time, and is therefore denoted "50% ON" in Figure 15. Initially, measurement of the output was recorded every second, but after several minutes the sampling interval was increased to 20 s so that one sample was taken every time the electrode was submerged, and no open circuit measurements were recorded. The raw data is shown in Figure 15(a). This test was repeated with a duty cycle of 10 s "on" and 20 s "off", which corresonds to an "on" time of one-third of the total time, and is thus denoted "33% ON". Unfortunately, during the second dip-test, the sampling and switching timing were different by some fraction of a second, so that, after several hours of experimentation, the sampling began occurring while the circuit was open. The discrepancy in the periods of the two processes continued to shift so that they alternated between in phase and out of phase multiple times. While out of phase the open circuit measurements were random and usually

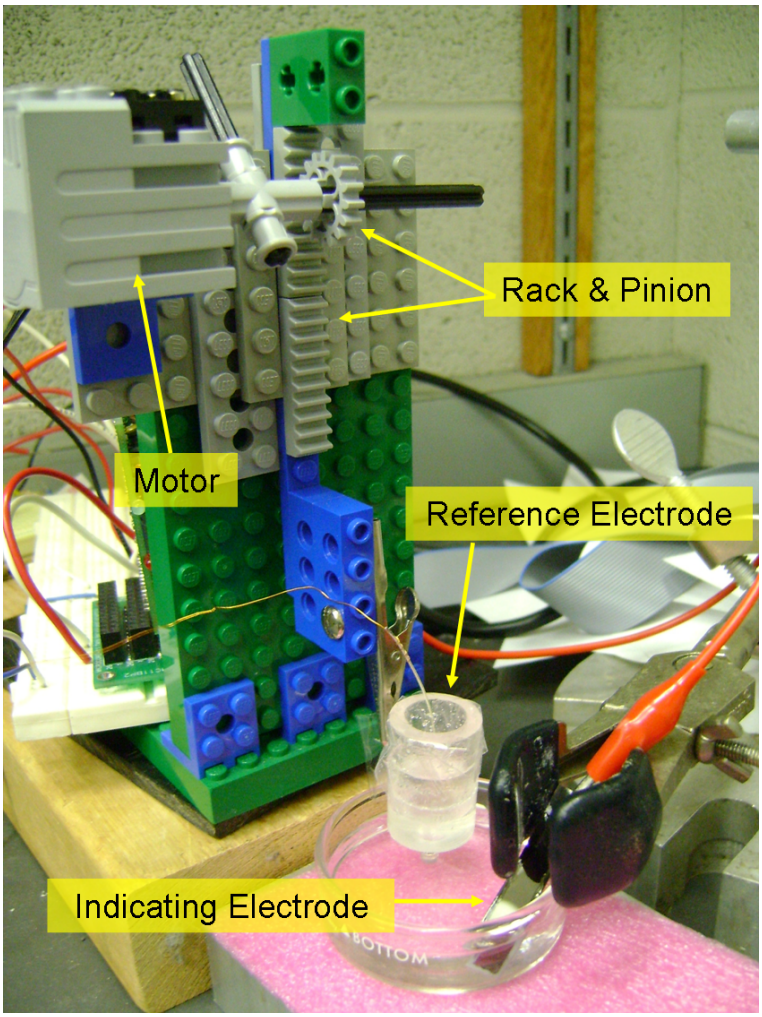

Figure 14: Experimental setup for switching simulation showing prototype reference electrode whose position is controlled by a motor connected to a rack and pinion.

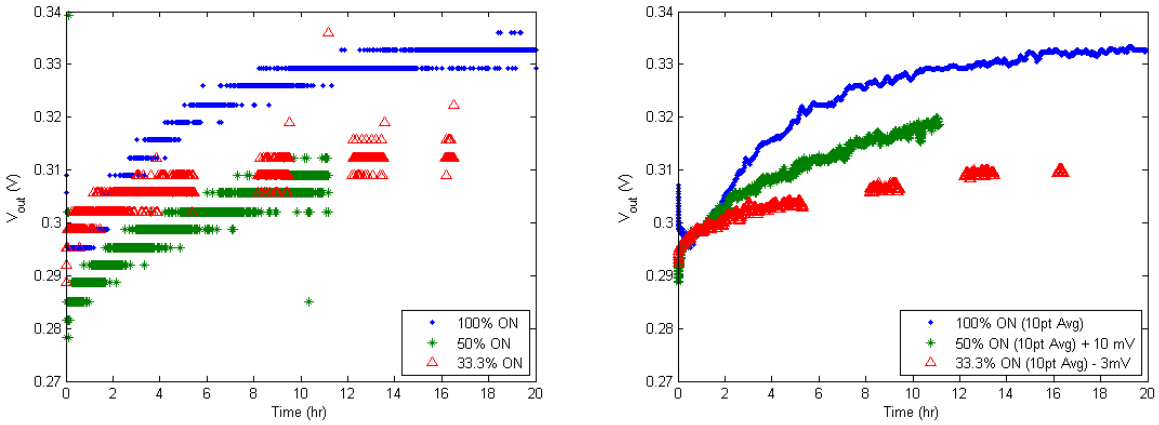

(a) Raw Data over relevant range.

(b) Processed data showing slower signal drift for smaller ON/OFF ratios

Figure 15: First experiment simulating the switching mechanism.

well out of the range of the in phase measurements. Thus, in Figure 15, there are gaps in the "33% ON" data. These open circuit measurements were removed from the data set. In addition, down-sampling was done on the early, high frequency sampled data in order to take a ten point moving average of the voltage data. This smoothed data was easier to compare graphically. Finally, small offsets were added to two of the data sets in order to make more clear the differences in rate of signal drift across tests. This processed data is shown in Figure 15(b). This figure clearly shows that the more time the sensor was in the "off" state, the slower the drift proceeded. This is proof that inclusion of a microfluidic switching mechanism has potential to extend sensor life.

The second set of tests were performed with two sputtered IrO_2 electrodes which had not been previously used. The first electrode was used to measure the pH of pH 7 buffer solution continuously for over 20 hours, taking 1 sample every minute. The second electrode performed the same task, but was interrupted for 50 s intervals every minutes, making a 1:5 ON/OFF ratio, or 16.7% ON time. This test was conducted for 60 hours. In Figure 16, both the raw and processed data of these tests are given. As the figure shows, the signal increases and then decreases. This behaviour was unexpected as all other tests have shown a change in only one direction, similar

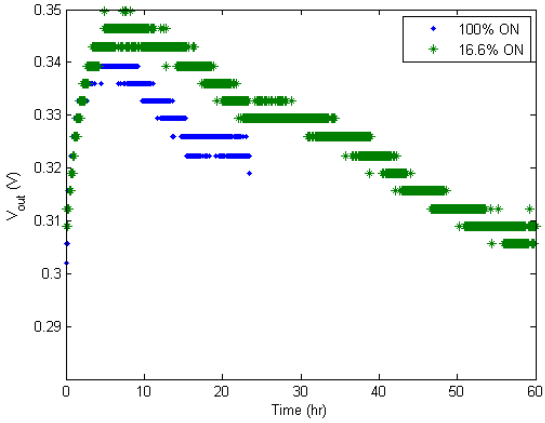

(a) Raw Data over relevant range.

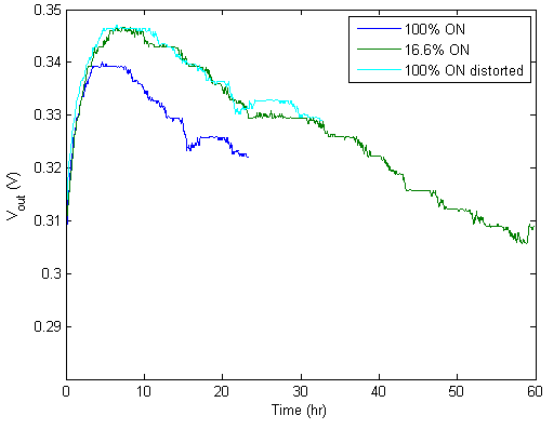

(b) Processed data showing extension of sensor time frame due to switching

Figure 16: Second experiment simulating the switching mechanism.

to the result presented in Figure 10. The cause of this is unknown and can only be attributed to the variety of histories amongst the electrodes. In addition, in Figure 16(b), a graph of the control (100% ON) test is distorted by multiplying the time vector of data points by 1.4, and offset by adding 7 mV to the voltage vector of data points. This was done to show that the switching mechanism extends the life of the sensor without otherwise affecting the sensor performance. This preliminary experiment shows an approximately 40% expansion of the time frame. Certainly, further improvements on this result are possible. For example, changing the absolute ON time, as compared to the ON/OFF ratio, may contribute significantly to the effect of switching.

3.5 Response Time

Another important factor is the response time of the sensor. A successful switching mechanism would extend sensor life based on the duty cycle, the "on-off ratio". Decreasing the time the sensor needs to be "on" to $\frac{1}{n}$ of the total time, increases the life of the sensor n times, theoretically. The

minimum “on” time is constrained by the response of the sensor, making this characteristic an important factor in determining the usefulness of a switching mechanism.

From the literature review, IrO_2 is expected to have a very fast response time which is inhibited when a Nafion® coating is added. In order to investigate the response time of the fabricated pH sensor, three buffer solutions were used to implement step changes in input. An AEIROF's response to each of these inputs was measured for over 3 min. The electrodes were submersed in pH 7, then pH 4, and finally pH 10 buffer solutions. The output is show in Figure 17, which shows responses for both coated and uncoated samples. (Some extraneous points may be noticed in the graph which are due to random floating voltages recorded while the circuit was open during the switch between solutions; these can be ignored.)

The uncoated sample responds almost instantly, while the Nafion® coated sample is noticeably slower, as expected. The duration of the response for the coated electrode is over 200 sec while Marzouk reported responses of no more than 90 sec [35]. There may be changes in fabrication which could improve this, but considering that the test presented is not a titration, which is beyond the experience level of the author, as is standard chemistry procedure for measuring response times, only a qualitative comparison should be made. The conclusion is that the response time with and without Nafion® tend to behave as predicted, thus results in the literature can safely be assumed to apply to the electrodes discussed here. Since in-situ testing may be a demanding environment, as the porcine blood tests suggested, a properly applied Nafion® coating seems to be a must, so that the slower response time must unfortunately be endured. The mininum “on time” for this Nafion coated IrO_2 sensor is then 200 sec.

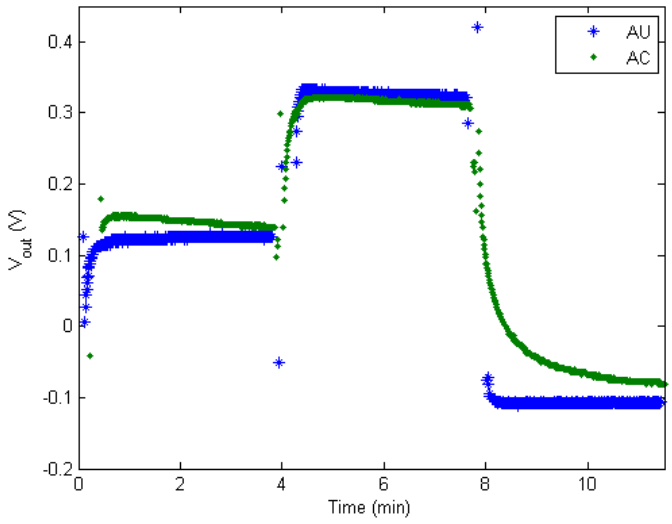

Figure 17: Response of Nafion® coated (AC) and uncoated (AU) AEIROF in pH 7 (0–4 min), pH 4 (4–8 min), and pH 10 (8–11.5 min) buffer solutions.

4.0 CONCLUSION

4.1 Summary of Results

Three types of fabrication techniques have been used to create IrO_2, which is sensitive to pH. Testing of electrodes with this ion sensitive layer was done with a Ag/AgCl reference electrode. The electrodes' response to pH was linear when tested in stable buffer solutions of pH 4, 7, and 10, but the AEIROF-based sensors showed appreciable error when tests were performed in heparanized porcine blood. The response of the electrochemically fabricated electrodes was super-Nernstian and of magnitudes that agreed with the literature. Sputtered electrodes showed near-Nernstian repsonses which also agreed with the literature. These results confirm the successful fabrication of pH sensors, though the AEIROF's, at least, proved not to be robust, indicating further improvement of the fabrication procedure is necessary.

Several life tests have been performed to show that a non-negligible amount of drift occurs in the pH sensors studied. The cause of the signal drift was not definitively isolated, but it has been shown that interrupting the electrochemical circuit of a pH sensor can delay this drift in signal output. Microfluidic switching is therefore a promising means of extending sensor life and further investigation is justified.

One significant difference between the switching simulation and actual micro-scale pH sensors, is the volume of inner electrolyte. Since one problem of the reference electrode is the leaching of ions through the liquid junction, a smaller volume would exacerbate the problem. Thus, the effect of the switching mechanism on this problem is not fully realized in the simulation presented here. The benefits of switching are expected to be significantly amplified in an actual micro-scale pH

sensor, as the switching mechanism addresses this problem directly. So it is fair to suppose that a more accurate simulation will show even more improvements of the switching case over the pH sensor without it.

4.2 Future Work

As was mentioned at various points in Chapter 3, there are several factors that affect the output of the fabricated sensors which may be of interest for further investigation. For example, the slope of the AEIROF response seemed to change merely from storage. Study of this behavior and contributing factors could reveal means of manipulating sensor life. Causes of the observed decay have not been proven, and the nature of the output after the first 20 hours may also be of interest for implantable devices. The unexpected trend in the final dip-test might warrant investigation. Of course, the precision and repeatability of the pH sensor in harsh environments needs to be improved as the blood tests revealed.

In order to further test the microfluidic switching device, a more accurate simulation is appropriate. Once planar fabrication of a Ag/AgCl reference electrode is learned, the complete micro-scale pH sensor of Figure 3 can be fabriacted by the researchers here in The University of Pittsburgh's Mechanical Engineering Department. This would directly enable study of reference electrode decay due to leaching of Cl^- ions from a microliter volume on inner electrolyte, for example.

There may be other improvements to pH sensors that microfluidics could offer. For example, an automated, on-site recalibration, as suggested by Bris and Birot [7], could conceivably be achieved for implantable devices using microfluidics.

The ultimate goal of this research direction has been to implement a microfluidic means of extending pH sensor life. All research to that end will have begun here, where it has been shown that switching can decrease signal drift. One question to examine before going forward is whether or not the choice of iridium oxide made here is superior to other options like the ISFET. The questions about its behavior raised here are daunting, and the need for a protective coating which

significantly delays the sensor response may, in itself, prevent iridium oxide from surmounting the pile of pH sensing technologies.

Finally, there are other opportunities for the use of a switching mechanism for extended sensor life that are applicable to micro-scale implanted biomedical use. For example, ion detecting sensors, like a pK^+ or pCO_2 sensors, may be able to adopt the switching mechanism with little or no changes from a device designed for the pH sensor. In summary, the microfluidic switching mechanism shows great potential for improving micro-scale biomedical devices.

BIBLIOGRAPHY

[1] Guidelines establishing test procedures for the analysis of pollutants under the clean water act; national primary drinking water regulations; and national secondary drinking water regulations; analysis and sampling procedures. http://www.epa.gov/EPA-WATER/2007/March/Day-12/w1073.htm, March 2007.

[2] Bruce Alberts, Alexander Johnson, Martin Raff, Keith Roberts, and Peter Walker. *Molecular Biology of the Cell*. Garland Science, Taylor and Francis Group, LLC, 5th edition, 2008.

[3] Ph. Arquint, B. H. van der Schoot, and N. F. de Rooij. Combined blood gas sensor for pO_2, pCO_2, and pH. *Proceeding μTAS '94 Workshop*, pages 191–194, 1994.

[4] T. C. Axford, J. A. Dearani, and I. Khait. Electrode-derived myocardial pH measurements reflect intracellular myocardial metabolism assessed by phosphorus 31-nuclear magnetic resonance spectroscopy during normothermic ischemia. *Journal of Thoracic and Cardiovascular Surgery*, 103:902–907, 1992.

[5] Roger G. Bates. *Determination of pH: Theory and Practice*. John Wiley & Sons, Inc., 1973.

[6] Mark H. Beers, Andrew J. Fletcher, Thomas V. Jones, and Robert Porter, editors. *Merck Manual of Medical Information*. POCKET BOOKS, a division of Simon and Schuster, Inc., second home edition, 2003. Published by arrangement with Merk and Co., Inc.

[7] N. Le Bris and D. Birot. In-situ pH measurement : a continuous flow analysis method for seawater pH determination using a ion sensitive field effect transistor (ISFET). pages 704–707, 1994.

[8] Denis N. Buckley, Laurence D. Burke, and Joseph K. Mulcahy. The oxygen electrode part 7. *Journal of the Chemical Society, Faraday Transactions 1: Physical Chemistry in Condensed Phases*, 72:1896–1902, 1976.

[9] Laurence D. Burke, Joseph K. Mulcahy, and David P. Whelan. Preparation of an oxidized iridium electrode and the variation of its potential with pH. *Journal of Electroanalytical Chemistry*, 163:117–128, 1984.

[10] Richard F. Burton. Defining and teaching pH. *Journal of Chemical Education*, 84(7):1129, July 2007.

[11] Sung Kwon Cho, Hyejin Moon, and Chang-Jin Kim. Creating, transporting, cutting, and merging liquid droplets by electrowetting-based actuation for digital microfluidic circuits. *Journal of Microelectromechanical Systems*, 12(1):70–80, February 2003.

[12] Sang Kug Chung and Sung Kwon Cho. On-chip manipulation of objects using mobile oscillating bubbles. *Journal of Micromechanics and Microengineering*, 18, 2008.

[13] Sang Kug Chung and Sung Kwon Cho. 3-d manipulation of millimeter- and micro-sized objects using an acoustically excited oscillating bubble. *Microfluidics and Nanofluidics*, 6:261–265, 2009.

[14] Sang Kug Chung, Yuejun Zhao, and Sung Kwon Cho. On-chip creation and elemination of microbubbles for a micro-object manipulator. *Journal of Micromechanics and Microengineering*, 18, 2008.

[15] A. K. Covington, P. D. Whalley, and W. Davison. Improvements in the precision of pH measurements, a laboratory reference electrode with renewable free-diffusion liquid junction. *Analytica Chimica Acta*, 169:221–229, 1985.

[16] René E. Dohner, Dorothée Wegmann, Werner E. Morf, and Wilhelm Simon. Reference electrode with free-flowing free-diffusion liquid junction. *Analytical Chemistry*, 58:2585–2589, 1986.

[17] W. D. Dozier, J. M. Drake, and J. Klafter. Self-diffusion of a molecule in porous vycor glass. *Physical Review Letters*, 56:197–200, 1986.

[18] Igor A. Ges, Borislav L. Ivanov, David K. Schaffer, Eduardo A. Lima, Andreas A. Werdich, and Franz J. Baudenbacher. Thin-film IrO_x pH microelectrode for microfluidic-based microsystems. *Biosensors and Bioelectronics*, 21(2):248–256, August 2005.

[19] Roy M. Harrison, editor. *Principles of Enviromental Chemistry*. RSC Publishing, 2007.

[20] J. Hendrikse, W. Olthuis, and P. Bergveld. A method of reducing oxygen induced drift in iridium oxide pH sensors. *Sensors and Actuators B*, 53:97–103, 1998.

[21] Michael L. Hitchman and Subramaniam Ramanathan. Evaluation of iridium oxide electrodes formed by potential cycling as pH probes. *Analyst*, 113:35–39, January 1988.

[22] Gwyneth Howells. *Acid Rain and Acid Waters*. Ellis Horwood, 2nd edition, 1995.

[23] I-Yu Huang and Ruey-Shing Huang. Fabrication and characterization of a new planar solid-state reference electode for ISFET sensors. *Thin Solid Films*, 406:255–261, 2002.

[24] Richard M. Hunt. Importance of pH control in the management of GERD. *Archives of Internal Medicine*, 159:649–657, April 1999.

[25] John A. Illingworth. A common source of error in pH measurements. *Biochemical Journal*, 195:259–262, 1981.

[26] David J. G. Ives and George J. Janz, editors. *Reference Electrodes, Theory and Practice*. Academic Press Inc., 1961.

[27] J. Janata. *Principles of Chemical Sensors*. Plenum, New York, 1989.

[28] Peter J. Kahrilas and Eamonn M. M. Quigley. Clinical esophageal pH recording: a technical review for practice guideline development. *Gastroenterology*, 110:1981–1996, 1996.

[29] B. K. Kapur, P. J. Howlett, N. G. Kenyon, M. J. Lunt, J. G. Mills, R. H. Smallwood, A. J. Wilson, and K. D. Brandhan. Continuous 24 hour ambulatory monitoring of intragastric pH in man. *Clinical Physics and Physiological Measurement*, 8:123–132, 1987.

[30] T. Katsube, I. Lauks, and J. N. Zemel. pH-sensitive sputtered iridium oxide films. *Sensors and Actuators*, 2:399–410, 1982.

[31] Patrick J. Kinlen, John E. Heider, and David E. Hubbard. A solid-state pH sensor based on a nafion-coated iridium oxide indicator electrode and a polymer-based silver chloride reference electrode. *Sensors and Actuators B*, 22:13–25, 1994.

[32] Kenneth G. Kreider, S. Semancik, and J. W. Erickson. Instability in pH measurements of sputtered IrO_2 films. *Transducers '87*, 1987.

[33] Kenneth G. Kreider, Michael J. Tarlov, and James P. Cline. Sputtered thin-film pH electodes of platinum, palladium, ruthenium, and iridium oxides. *Sensors and Actuators B*, 28:167–172, 1995.

[34] Harvey Lodish, Arnold Berk, S. Lawrence Zipursky, Paul Matsudaira, David Baltimore, and James Darnell. *Molecular Cell Biology*. W. H. Freeman and Company, 4th edition, 2000.

[35] Sayed A. M. Marzouk. Improved electrodeposited iridium oxide pH sensor fabrication on etched titanium substrates. *Analytical Chemistry*, 75(6):1258–1266, March 2003.

[36] Sayed A. M. Marzouk, Stefan Ufer, and Richard P. Buck. Electrodeposited iridium oxide pH electrode for measurement of extracellular myocardial acidosis during acute ischemia. *Analytical Chemistry*, 70(23):5054–5061, December 1998.

[37] Donald A. McQuarrie. *Mathematical Methods for Scientists and Engineers*. University Science Books, 2003.

[38] D. Midgley and K. Torrance. An assessment of various types of reference electrode for use in continuous potentiometric analysis with particular application to highly pure waters. *The Analyst*, 101(1208):833–847, November 1976.

[39] F. Moussy and D. J. Harrison. Prevention of the rapid degradation of subcutaneously implanted Ag/AgCl reference electrodes using polymer coatings. *Analytical Chemistry*, 66:674–679, 1994.

[40] M. A. Nolan, S. H. Tan, and S. P. Kounaves. Fabrication and characterization of a solid state reference electrode for electroanalysis of natural waters with ultramicroelectrodes. *Analytical Chemistry*, 69:1244–1247, 1997.

[41] W. Olthuis, M. A. M. Robben, P. Bergveld, M. Bos, and W. E. van der Linden. pH sensor properties of electrochemically grown iridium oxide. *Sensors and Actuators B*, 2:247–256, 1990.

[42] Mohammad Pessarakli, editor. *Handbook of Plant and Crop Stress*. Marcel Dekker Inc., 2nd edition, 1999.

[43] Peter G. Pickup and V.I. Birss. A model for anodic hydrous oxide growth at iridium. *Journal of Electroanalytical Chemistry*, 220:83–100, 1987.

[44] L. M. Schiavone, W. C. Dautremont-Smith, G. Beni, and J. L. Shay. Electrochromic iridium oxide films prepared by reactive sputtering. *Applied Physics Letters*, 35(10):823–825, 1979.

[45] Paul Shewmon. *Diffusion in Solids*. The Minerals, Metals and Materials Society, 1989.

[46] Anette Simonis, Marek Dawgul, Hans Lüth, and Michael J Schöning. Miniaturised reference electrodes for field-effect sensors compatible to silicon chip technology. *Electrochimica Acta*, 51:930–937, 2005.

[47] R. L. Smith and D. C. Scott. An integrated sensor for electrochemical measurements. *IEEE Transactions on Biomedical Engineering*, BME-33(2):83–90, February 1986.

[48] Hiroaki Suzuki, Taishi Hirakawa, Satoshi Sasaki, and Isao Karube. Micromachined liquid-junction Ag/AgCl reference electrode. *Sensors and Actuators B*, 46:146–154, 1998.

[49] Hiroaki Suzuki, Atsunori Hiratsuka, Satoshi Sasaki, and Isao Karube. Problems associated with the thin-film Ag/AgCl reference electrode and a novel structure with improved durability. *Sensors and Actuators B*, 46:104–113, 1998.

[50] Michael J. Tarlov, S. Semancik, and Kenneth G. Kreider. Mechanistic and response studies of iridium oxide pH sensors. *Sensors and Actuators B*, 1:293–297, 1990.

[51] B. H. van der Schoot, P. Bergveld, M. Bos, and L. J. Bousse. The ISFET in anlytical chemistry. *Sensors and Actuators*, 4:267–272, 1983.

[52] Gail Vaughn. *Understanding and Evaluating Common Laboratory Test*. Appleton and Lange, 1999.

[53] K. Yamanaka. Anodically electrodeposited iridium oxide films (AEIROF) from alkaline solutions for electrochromic display devices. *Japanese Journal of Applied Physics, Part 1 (Regular Papers & Short Notes)*, 28(4):632–637, April 1989.

[54] Yuejun Zhao and Sung Kwon Cho. Microparticle sampling by electrowetting-actuated droplet sweeping. *Lab on a Chip*, 6:137–144, 2006.

[55] Yuejun Zhao and Sung Kwon Cho. Droplet manipulation on high-opening micro filter meshes. *2008 IEEE 21st International Conference on Micro Electromechanical Systems - MEMS 2009*, 2008.